Applied Thermal Engineering 56 (2013) 62–76

Contents lists available at SciVerse ScienceDirect

Applied Thermal Engineering

journal homepage: www.elsevier.com/locate/apthermeng

On a computational study for investigating acoustic streaming and heating during focused ultrasound ablation of liver tumor

Maxim A. Solovchuk [a,b], Tony W.H. Sheu [a,b,c,*], Marc Thiriet [d], Win-Li Lin [e]

[a] Department of Engineering Science and Ocean Engineering, National Taiwan University, No. 1, Sec. 4, Roosevelt Road, Taipei 10617, Taiwan, ROC
[b] Center of Advanced Study in Theoretical Science (CASTS), National Taiwan University, Taiwan, ROC
[c] Department of Mathematics, National Taiwan University, Taiwan, ROC
[d] LJLL, University of Paris # 6, Paris, France
[e] Institute of Biomedical Engineering, National Taiwan University, Taiwan, ROC

HIGHLIGHTS

- 3D three-field coupling physical model for focused ultrasound tumor ablation is presented.
- Acoustic streaming and blood flow cooling effects on ultrasound heating are investigated.
- Acoustic streaming can considerably affect the temperature distribution.
- The lesion can be reduced by 30% due to the acoustic streaming effect.
- Temperature on the blood vessel wall is reduced by 54% due to the acoustic streaming effect.

ARTICLE INFO

Article history:
Received 16 October 2012
Accepted 26 February 2013
Available online 28 March 2013

Keywords:
HIFU
Liver tumor
Acoustic streaming
Heating
Navier–Stokes equations

ABSTRACT

The influences of blood vessels and focused location on temperature distribution during high-intensity focused ultrasound (HIFU) ablation of liver tumors are studied numerically. A three-dimensional acoustics-thermal-fluid coupling model is employed to compute the temperature field in the hepatic cancerous region. The model construction is based on the linear Westervelt and bioheat equations as well as the nonlinear Navier–Stokes equations for the liver parenchyma and blood vessels. The effect of acoustic streaming is also taken into account in the present HIFU simulation study. Different blood vessel diameters and focal point locations were investigated. We found from this three-dimensional numerical study that in large blood vessels both the convective cooling and acoustic streaming can considerably change the temperature field and the thermal lesion near blood vessels. If the blood vessel is located within the beam width, both acoustic streaming and blood flow cooling effects should be addressed. The temperature rise on the blood vessel wall generated by a 1.0 MHz focused ultrasound transducer with the focal intensity 327 W/cm^2 was 54% lower when acoustic streaming effect was taken into account. Subject to the applied acoustic power the streaming velocity in a 3 mm blood vessel is 12 cm/s. Thirty percent of the necrosed volume can be reduced, when taking into account the acoustic streaming effect.

1. Introduction

High intensity focused ultrasound (HIFU) is a rapidly developing medical technology for conducting a non-invasive tumor ablation surgery. HIFU therapy has been successfully applied to treat solid malignant tumors in different areas of the body, including the prostate, breast, liver, pancreas, uterine fibroids [1–3]. The absorbed ultrasound energy in tissue is transformed into the thermal energy during focused therapy and this energy deposition can quickly elevate the tissue temperature. With the ultrasound beam being focused, thermal energy can be added primarily to a small region of tissues with little or no deposition at all on the surrounding tissues. When tissue temperature is higher than 55 °C, thermal coagulation necrosis occurs [4]. Temperatures above 95 °C can lead to tissue boiling and cavitation and can cause undefined and unpredictable lesion growth [4–6]. For the ablation of large tumor volumes consecutive single sonications should be combined without a gap until the whole tumor is ablated.

* Corresponding author. Department of Engineering Science and Ocean Engineering, National Taiwan University, No. 1, Sec. 4, Roosevelt Road, Taipei 10617, Taiwan, ROC. Tel.: +886 2 33664429.
E-mail addresses: solovchuk@gmail.com, solovchuk@yandex.ru (M.A. Solovchuk), twhsheu@ntu.edu.tw (T.W.H. Sheu).

1359-4311/$ – see front matter © 2013 Elsevier Ltd. All rights reserved.
http://dx.doi.org/10.1016/j.applthermaleng.2013.02.041

Nomenclature

c_0	speed of ultrasound in tissue, m/s
c	specific heat, J/kg °C
$\underline{\mathbf{F}}$	force vector per unit volume, N/m^3
k	wave number
k_t	thermal conductivity of tissue, W/m °C
I	sound intensity, W/m^2
p	acoustic pressure, N/m^2
$\mathbf{P}$	fluid static pressure, N/m^2
q	ultrasound power deposition, W/m^3
t	time, s
t_0	initial time, s
t_{final}	final time, s
T	temperature, °C
u	blood flow velocity, m/s
w	velocity in z direction, m/s
w_b	blood perfusion rate, kg/m^3 s
x	coordinate in the x direction
y	coordinate in the y direction
z	coordinate in the z direction

Greek symbols

α	absorption coefficient, Np/MHz m
β	nonlinearity coefficient
δ	acoustic diffusivity
λ	wavelength, m
μ	shear viscosity of blood flow, kg/m s
ψ	acoustic velocity potential
ω	angular frequency, MHz

Subscripts

t	tissue
b	blood

Liver cancer is the second leading cause of death in Asia [7] and is now known as one of the most leading causes of death in the world. There are three major blood vessels in liver: hepatic artery, portal vein and hepatic vein. If the vital blood vessels adjacent to the tumors are severely damaged during the treatment, lethal complications may develop. Special care should be taken to avoid destruction of the vessel wall by a high temperature [8,9]. Quite recently [10] it was first shown that HIFU can safely necrotize the tumors close to major hepatic veins. Before HIFU treatment some patients had transcatheter chemoembolization. After a single session of HIFU treatment, the rate of complete necrosis was about 50%, which is not satisfactory at all. Lack of a complete response can be attributed to the large tumor size and the cooling effect in large vessels. Large blood vessels (hepatic arteries, hepatic veins and portal veins) act as heat sink. Convective cooling can reduce the necrosed volume and cause consequently the recurrent cancer. A basic understanding of the factors that can influence altogether the tissue necrosis volume is necessary to improve thermoablative therapy and prevent recurrence.

Temperature elevation in soft tissues is mostly modeled by the well-known Pennes bioheat transfer equation. Within this analysis framework, the heat source is produced by the incident acoustic wave and heat sink owing to the perfusion in capillaries [11]. Blood vessels are considered to be in thermal equilibrium with tissue. The amount of dissipated heat is estimated by averaging the effect of blood perfusion over all tissues. This approach is valid for tissues with capillaries. However, for tissues with thermally significant blood vessels (diameters larger than 0.5 mm) the biologically relevant convective cooling needs to be taken into account, and homogenization assumption is no longer valid [12–16]. The biologically relevant convective cooling in large blood vessels and perfusion cooling in the microvasculature need to be taken into account altogether. Inclusion of these two possible cooling means will greatly increase the modeling complexity since the equations of motion for blood flow need to be solved together with the divergence-free velocity constraint equation. Kolios et al. [13] and Curra et al. [17] studied the influence of blood vessel on the lesion size. The temperature elevation during focused ultrasound surgery was computed by two coupled bioheat equations, one for the tissue domain, that contains blood vessels with the diameter $<$0.5 mm, and the other for the blood domain in thermally significant blood vessels. The blood vessel was on the acoustic axis. They carried out a 2D finite difference calculation in cylindrical coordinate system. The focal point was at the center of blood vessel. In this case a large part of the deposited ultrasound energy was carried away by the convective cooling and ablation of tissue was complicated. Hariharan et al. [14] presented a 3D model to determine the influence of blood flow on the temperature distribution. Their model was constructed on the basis of the acoustic and bioheat equations. They neglected the heat source inside the blood vessel. It was based on the assumption that the blood vessel is outside the 6 dB width of the beam (half pressure maximum width), which can be considered as an estimation of the lesion width. When the tumor is in close proximity to the blood vessel, their model cannot be applied. They considered uniform velocity distribution in the blood vessel. For real blood vessel geometry it is necessary to solve the nonlinear hemodynamic equations to get a better predicted velocity distribution.

Ultrasound propagating in a viscous fluid can induce an additional mass flow. This effect is known as the acoustic streaming. Acoustic streaming has been observed in cyst fluid in breast, ovary and testicle. Streaming has been suggested as a diagnostic tool to differentiate cysts from solid lesions [18]. Detection of streaming can help to improve hemorrhage diagnosis. Acoustic streaming can be used to characterize high intensity focused ultrasound transducers [19]. Acoustic streaming plays a significant role in microfluidic devices, manipulating both fluids and particles within those fluids at the microscale and nanoscale [20].

Acoustic streaming was first investigated by Rayleigh [21], who studied circulation of air observed in Kundt's tubes. Later Eckart [22] theoretically studied the acoustic streaming profiles generated by the uniform cylindrical ultrasound beam in an infinite circular tube. The beam has a much smaller width than the tube diameter. He considered linear Navier–Stokes equations at the steady-state. Perelomova [23] developed projecting method to study the effects of acoustic heating and acoustic streaming. Analytical results of the earlier studies [22,24,25] cannot be applied to predict the acoustic streaming velocities in blood vessels during HIFU therapy [26]. Acoustic streaming induced by diagnostic B-scan transducers and scanned diagnostic arrays have been investigated both theoretically and experimentally [27,28]. Diagnostic ultrasound transducer induced acoustic streaming velocities up to 15 cm/s [27]. Streaming velocities inside blood vessels or other confined volumes are expected to be much lower [29,30]. Starritt et al. [31] used MRI to visualize the streaming in confined volumes and concluded that in small volumes detectable streaming occurs at very low power levels. Wu et al. [32] showed in in-vitro experiments that acoustic streaming in a liquid may dramatically reduce the temperature rise generated by ultrasound at the bone surface, if the ultrasound path contain the liquid in contact with the bone. Layman et al. [33] investigated experimentally the unsteady heating and acoustic

streaming generated by a high-intensity acoustic horn in a thermo-viscous fluid for sonochemical applications. Authors [33,34] indicated a great need of the theoretical analysis of the acoustic streaming effect on ultrasonic heating. To the best of the authors' knowledge, numerical result, which is computed from the heat transfer equation for a large blood vessel and its surrounding tissue together with the nonlinear hemodynamic equations with an acoustic streaming effect, has not yet been reported for the simulation of HIFU tumor ablation. The whole physics remains nowadays poorly understood. Multiphysics modeling for the description of interactions between fluid dynamics, acoustic field and thermal field is highly desirable. The three dimensional acoustics-thermal-fluid mathematical model presented in Ref. [16] took the less explored acoustic streaming effect into account. In Ref. [16] the model was applied to the patient specific liver geometry. In the current study different blood vessel diameters and blood vessel orientations are considered. The aim of this work is to investigate the coupled effect of blood flow cooling and acoustic streaming on the temperature elevation and lesion size during focused ultrasound therapy. Such an analysis should be helpful to get a fundamental understanding of the biophysical effects of therapeutic ultrasound and factors that can influence the tissue necrosis volume. This information can be used in the treatment planning.

2. Methods

2.1. Three-field coupling mathematical model

2.1.1. Acoustic equation for ultrasound propagation

The Westervelt wave equation [35] given below for ultrasound pressure p will be employed to model the finite-amplitude nonlinear wave propagation in a soft tissue, which is modeled as a thermo-viscous fluid

$$\nabla^2 p - \frac{1}{c_0^2}\frac{\partial^2 p}{\partial t^2} + \frac{\delta}{c_0^4}\frac{\partial^3 p}{\partial t^3} + \frac{\beta}{\rho_0 c_0^4}\frac{\partial^2 p^2}{\partial t^2} = 0. \tag{1}$$

The first two terms describe the linear lossless wave propagating at a small-signal sound speed. The third loss term is due to thermal conductivity and fluid viscosity. The last term represents the acoustic nonlinearity which can affect the thermal and mechanical changes within tissues [36]. In soft tissues, which are assumed to be thermoviscous, the acoustic diffusivity δ accounts for the thermal and viscous losses in a fluid and is modeled by

$$\delta = \frac{2c_0^3\alpha}{\omega^2}. \tag{2}$$

In the above, α denotes the acoustic absorption coefficient. In Equation (1), $\beta = 1 + B/2A$ and ω ($\equiv 2\pi f$) are the nonlinearity coefficient and the angular frequency, respectively.

In the current HIFU simulation, the nonlinear acoustic effect, which will be the focus of our near future study, is neglected for simplifying the analysis within the linear context. In our study each small element dS of the transducer surface is assumed to vibrate continuously with the same velocity $u = u_0\exp(i\omega t)$ in the direction normal to the surface. The resulting linear wave equation $\nabla^2 p - (1/c_0^2)\partial^2 p/\partial t^2 + (\delta/c_0^4)\partial^3 p/\partial t^3 = 0$ is transformed to the diffraction integral for the velocity potential as follows [37,38]

$$\psi_P = \iint_S \frac{U}{2\pi r}\exp[-(\alpha + ik)r]\mathrm{d}S. \tag{3}$$

In the above, r denotes the distance from the source point on the transducer surface dS to a field point $\bar{p}$, and k is the wave number.

The pressure amplitude at $\bar{p}$ can be calculated from the following expression

$$p_{\bar{p}} = ikc\rho_t\psi, \tag{4}$$

where ρ_t is the density of tissues, and c is the speed of ultrasound in tissues. The ultrasound power deposition per unit volume given below is assumed to be proportional to the local acoustic intensity I

$$q = 2\alpha I. \tag{5}$$

In the above the intensity I is defined as

$$I = \frac{p^2}{2\rho_t c}. \tag{6}$$

Note that Equations (3) and (4) consider only the effects of diffraction and attenuation without taking the effect of nonlinearity into account. Several studies [5,19,29,36,39,40] showed that for the focal intensity in the range of 100–1000 W/cm^2 and the peak pressure smaller than 4 MPa, the physical complexities due to cavitation and nonlinearity field can be neglected with acceptable errors. If cavitation and acoustic nonlinearities are avoided, the lesion size and shape can be well predicted solely from the thermal consideration. In the present study the acoustic energy emitted from the transducer is 80 W. The intensity generated at the focus is 327 W/cm^2 and the pressure at the focal point is 3.27 MPa. Therefore we don't consider here the effects of nonlinearity and cavitation.

2.1.2. Thermal energy equation for tissue heating

In this paper a biologically realistic thermal model will be developed by dividing the region of current interest into the region with tissue perfusion, which is attributed mainly to the capillary beds, and the capillary region containing blood vessels. In other words, the temperature field has been split into the domains for the perfused tissues, that contain blood vessels with the diameter <0.5 mm, and the flowing blood domain in thermally significant blood vessels.

In a region free of large blood vessels, the diffusion-type Pennes bioheat equation [11] given below will be employed to model the transfer of heat in the perfused tissue region:

$$\rho_t c_t\frac{\partial T}{\partial t} = k_t\nabla^2 T - w_b c_b(T - T_\infty) + q. \tag{7}$$

In the above energy equation, ρ, c, k denote the density, specific heat, and thermal conductivity, respectively. The subscripts t and b refer to the tissue and blood domains. The notation T_∞ is denoted as the temperature at a location that is quite far from the heating focus. For w_b ($\equiv 10$ kg/m^3 s) shown in Equation (7), it is known as the perfusion rate for the tissue cooling in capillary flows. It is noted that the above energy equation for T is coupled with the linear acoustic equation (4) for the acoustic pressure through the power deposition term q defined in Equation (5).

In the region containing large vessels, within which blood flow can convect heat, the biologically relevant heat source, which is q, and the heat sink, which is $-\rho_b c_b \underline{\mathbf{u}}\cdot\nabla T$, are added to the conventional diffusion-type heat equation. The resulting model equation can avoid a possible high recurrence

$$\rho_b c_b\frac{\partial T}{\partial t} = k_b\nabla^2 T - \rho_b c_b \underline{\mathbf{u}}\cdot\nabla T + q, \tag{8}$$

where $\underline{\mathbf{u}}$ is the blood flow velocity. In the presence of velocity vector $\underline{\mathbf{u}}$ in energy equation, we know that a biologically proper model for HIFU simulation comprises a coupled system of thermal-fluid-acoustics nonlinear differential equations. The heat sink has

Table 1
Acoustic and thermal properties for the liver tissue and blood.

Tissue	C_0, m/s	ρ, kg/m^3	c, J/kg K	K, W/mK	α, Np/m
Liver	1550	1055	3600	0.512	9
Blood	1540	1060	3770	0.53	1.5

association with the hydrodynamic equations that will be described in the following section. The heat source is governed by the acoustic field equation described in the previous section.

Thermal dose developed by Sapareto and Dewey [41] will be applied to get a quantitative relationship between the temperature and time for the heating of tissues and the extent of cell killing. In focused ultrasound surgery (the involved temperature is generally above 50 °C), the expression for the thermal dose (TD) can be written as

$$\mathrm{TD} = \int_{t_0}^{t_{\mathrm{final}}} R^{(T-43)}\mathrm{d}t \approx \sum_{t_0}^{t_{\mathrm{final}}} R^{(T-43)}\Delta t, \tag{9}$$

where $R = 2$ for $T \geq 43$ °C, and $R = 4$ for 37 °C $< T <$ 43 °C. The value of TD required for getting a total necrosis ranges from 25 to 240 min in biological tissues [34,41]. According to this relation, thermal dose resulting from the heating of tissues to 43 °C for 240 min is equivalent to that achieved by heating tissues to 56 °C for 1 s.

2.1.3. Acoustic streaming hydrodynamic equations

When blood vessel is located within a beam width of high-intensity ultrasound beam, according to Equation (8) the temperature in the tumor can be changed significantly depending on the blood flow velocity. High-intensity ultrasound beam can alter blood flow velocity; therefore we will include the effect of acoustic streaming in our mathematical model.

In this study we consider that the flow in large blood vessels is incompressible and laminar. The vector equation for modeling the blood flow motion, subject to the divergence free constraint equation $\nabla\cdot\underline{\mathbf{u}} = 0$, in the presence of acoustic stress vector $\underline{\mathbf{F}}$ is as follows [42]

$$\frac{\partial\underline{\mathbf{u}}}{\partial t} + \left(\underline{\mathbf{u}}\cdot\nabla\right)\underline{\mathbf{u}} = \frac{\mu}{\rho}\nabla^2\underline{\mathbf{u}} - \frac{1}{\rho}\nabla\mathbf{P} + \frac{1}{\rho}\underline{\mathbf{F}}. \tag{10}$$

In the above, $\mathbf{P}$ is the static pressure, μ (=0.0035 kg/m s) the shear viscosity of blood flow, and ρ the blood density. In Equation (10), the vector $\underline{\mathbf{F}}$ acting on the blood fluid due to ultrasound is assumed to propagate along the acoustic axis $\underline{\mathbf{n}}$. The resulting nonzero component of $\underline{\mathbf{F}}$ along the direction $\underline{\mathbf{n}}$ takes the following form [25]

$$\underline{\mathbf{F}}\cdot\underline{\mathbf{n}} = \frac{2\alpha}{c_0}I. \tag{11}$$

The acoustic intensity I shown above has been defined in Equation (6). Amongst the second-order physical effects, only the acoustic streaming will be taken into account.

2.2. Problem description

The single element HIFU transducer used in this study is spherically focused with an aperture of 12 cm and a focal length of 12 cm. This transducer presumably emits a beam of spherically-shaped ultrasound wave propagating toward the targeted tissue under the current investigation. The parameters used in the current simulation are listed in Table 1 [16,43].

Here we consider the case with the attenuation coefficient that is linearly dependent on the frequency [43]. In this study, the ultrasound of 1.0 MHz insonation is incident from a location that is exterior of the liver tumor. Typically, the duration of energy delivery ranges from 5 to 12 s [1,3]. The solid tumor was assumed to be exposed to an 8 s ultrasound. The acoustic energy is 80 W. In the current study we considered two blood vessel orientations: parallel and perpendicular to the acoustic axis (schematic in Fig. 1). The portal vein and hepatic vein have diameters up to 10–12 mm, the hepatic arteries have a diameter less than 3–4 mm [8,9,44]. The diameters of portal vein and hepatic vein are much larger than the diameter of hepatic artery. Usually, blood vessels with diameters from 0.5 mm to 6 mm are studied [13–15,45–48]. In Ref. [9] the effect of vessel size on the creation of hepatic radiofrequency lesions in pigs was studied for blood vessel diameters up to 10 mm. In this study blood vessel diameters ranging from 1.0 mm to 6.0 mm are investigated. Non-Newtonian blood flow is implemented in the model and the shear thinning effect is taken into account [49]. Shear thinning effect becomes important in tiny blood vessels [49]. For diameters larger than 1 mm considered in this article, shear thinning effect can be neglected. We calculated the axial velocity profiles for the Newtonian and non-Newtonian fluids for the geometry of the problem investigated in the current paper. The difference for the axial velocity profiles was less than 5–10%. Therefore to save computational time blood is considered as a Newtonian fluid in the current work. The blood viscosity is 0.0035 kg/(m s). The fully developed velocity profile is applied at the inlet of blood vessel, while zero gradient velocity boundary condition on the outlet plane. A no-slip boundary condition is applied on the vessel wall. Numerical results showed that the difference of lesion predicted for different inlet velocity profiles, pulsatile and parabolic, is very small [15,50].

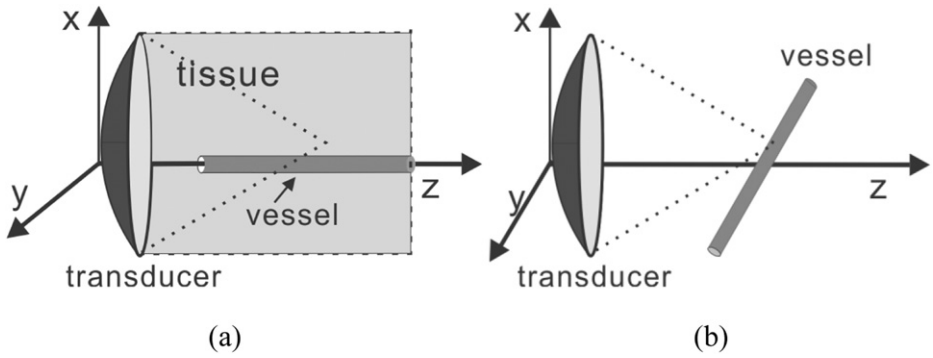

Fig. 1. Schematic of the physical models. (a) Blood vessel is parallel to the acoustics axis. The space enclosed by the dashed line and the transducer is the domain for conducting the current acoustic wave simulation. (b) Blood vessel is perpendicular to the acoustics axis.

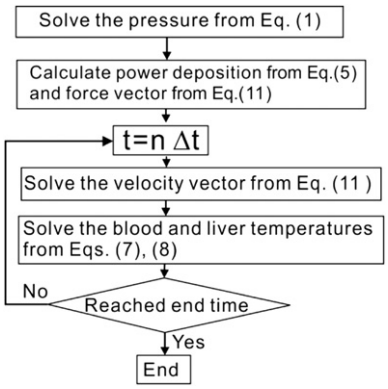

Fig. 2. Flow chart of the computational program.

2.3. Simulation model

Flow chart of the computational program is presented in Fig. 2. First the acoustic pressure was calculated. The acoustic pressure was calculated only once for a given set of transducer parameters. Afterward ultrasound power deposition in Equation (5) and acoustic streaming force in Equation (11) were determined and stored. Blood flow velocity was computed from Equation (10) at every time step with the acoustic streaming effect being taken into account and then substituted to the bioheat equation (8). With known blood flow velocities and power deposition terms, temperatures in blood flow domain and in liver were calculated. Initially, we consider that the temperature is equal to 37 °C. On the wall a constant temperature of 37 °C was prescribed. Temperature continuity at the fluid–solid interface is imposed as that applied in a conjugate heat transfer problem. The interface boundary condition takes into account thermal conduction in liver and convection in blood vessel domain.

The three-dimensional problem is analyzed using the commercially available CFDRC (CFDRC Research, Huntsville, AL, USA) software. A detailed description of the solution procedures can be found in our previous article [16]. For the calculation of temperature and velocity fields the computational domain has the dimensions of 6 cm × 4 cm × 4 cm. It is sufficient for the considered treatment time. In the focal region (3 mm × 3 mm × 20 mm) the refined grids were generated with a mesh size of 0.2 mm × 0.2 mm × 0.4 mm. The number of grids used in this study varies from 450 000 to 720 000 for different blood vessel diameters and blood vessel orientations. Mesh independence was carried out by comparing the temperature and velocity distributions in the final working mesh with the temperature and velocity obtained in a refined mesh (Fig. 3), which is generated by increasing the number of cells by 50%. In these two meshes, the temperatures and velocities differ from each other only by an amount less than 0.5%.

2.4. Comparison with the experimental data

In order to verify the theoretical analysis, experimental measurements were carried out in the following setting. The acoustic source and hydrophone were immersed in filtered and deionized water that is contained in a 74.5-cm-long, 36-cm-wide, and 50-cm-high tank, which is open to the atmosphere. A three-dimensional computerized positioning system is used to move the transducer along the beam axis and orthogonal directions. A single-element transducer has a focal length of 120 mm, an aperture of 120 mm, and frequency of 1.0 MHz. The transducer was driven by a continuous wave.

In Fig. 4, the measured pressure profile is plotted against the axial distances (in the focal plane). The solid lines and open circles correspond to the prediction and measurement results, respectively. These results were obtained in water at 25 °C using the chosen 0.4 mm hydrophone (Onda HNA-0400). The efficiency of the employed transducer was measured using the radiation force balance method. The electric energy of the transducer is equal to 1.9 W. The measured acoustic pressures are normalized by the focal pressure of 0.72 MPa. Good agreement between the measured and numerical results can be seen. Since power deposition is quadratic in pressure, the deviation between the measurement and model analysis in the low amplitude regions is not deemed significant.

3. Results and discussion

3.1. Validation of numerical model

Our three-dimensional computational model for the prediction of acoustic streaming field was validated by comparing the results with those of Kamakura et al. [42]. In Fig. 5(a) the streaming velocity profile is presented as the function of time at the focal point. Acoustic streaming is generated by the transducer with a Gaussian amplitude distribution, radius of 1 cm, 5-cm focal length, frequency 5 MHz, and maximum source pressure amplitude 30 kPa. The

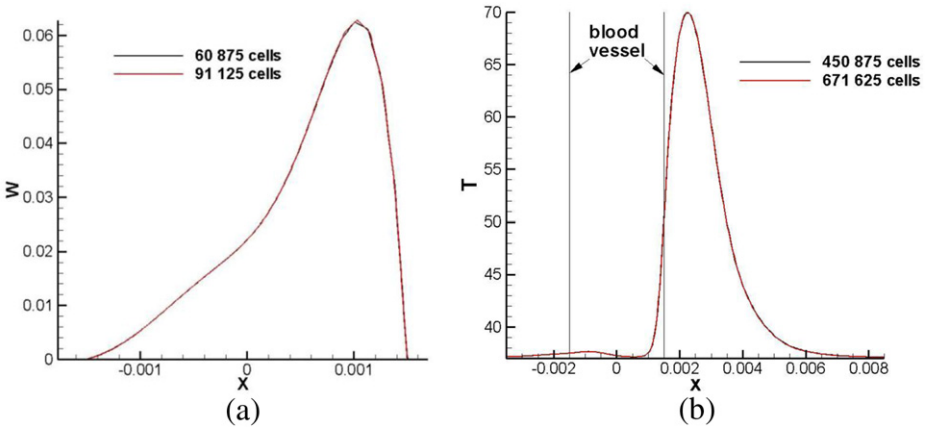

Fig. 3. Mesh independence study, parallel blood flow, $u = 0.016$ m/s, $d = 3$ mm, gap $= 0.5$ mm. (a) The simulated velocity profiles $w(x,y = 0,z = 0.12$ m) in the blood vessel at the focal plane with acoustic streaming effect being taken into account; (b) the predicted temperature distributions at $t = 8$ s along x (axial distance) direction using two different cell numbers.

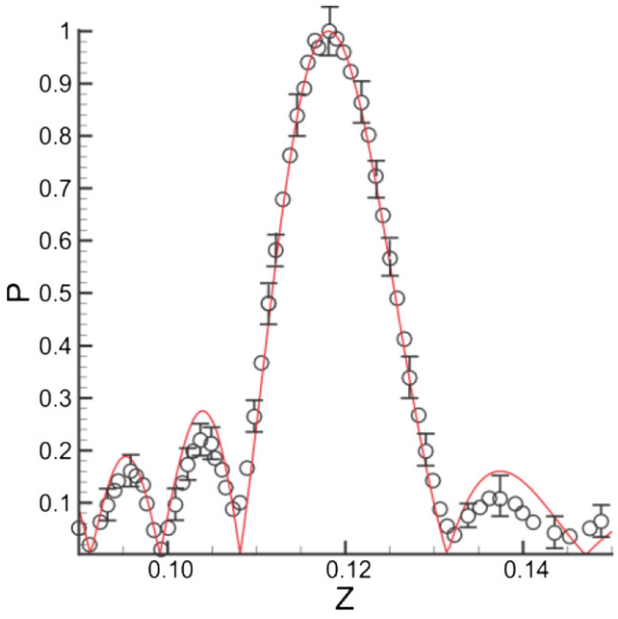

Fig. 4. The measured (circle) and computed (solid line) normalized pressure profiles in water at 0.72 MPa focal pressure.

difference between our 3D-model result and the 2D-model result of Kamakura et al. (Fig. 2 of Kamakura et al. [42]) is less than 1%.

The present computational model was also validated by comparing our simulated results with the experimental results of Huang et al. (Fig. 4 of Huang et al. [45]) in Fig. 5(b). This comparison was made for the temperature field in a uniform phantom. The simulation results include the thermocouple artifact heating. The acoustic frequency, peak focal pressure, and sonication time were 1.0 MHz, 1.11 MPa, and 1 s, respectively. The transducer radius was 7 cm, and the focal length is 6.3 cm. Our results are in good agreement with the experimental data.

Then we compare the calculated temperature fields with the experimental results of Huang et al. (Fig. 8 of Huang et al. [45]) in a tissue phantom with 2.6 mm blood vessel. Our results presented in Fig. 5(c) have good agreement with the experimental data of Huang et al. (Fig. 8 of Huang et al. [45]) for the mean flow velocities of 0 and 1.87 cm/s within the estimated uncertainties in the temperature measurements.

3.2. Effect of convective cooling on the temperature distribution for different blood vessel orientations

In this section we will study the temperature distribution in liver, when the distance between the focal point and blood vessel is 1.0 mm. The blood vessel is parallel to the acoustic axis. The vessel diameter is 3 mm. At inlet, the blood flow cross-sectional average velocities are set at 0.016 m/s and 0.13 m/s, that correspond to the velocities in veins and liver arteries with diameter 3 mm [51].

In Fig. 6 we can see the computed temperature contours at $t = 8$ s in the liver at the cutting planes $y = 0$ and $z = 0.12$ for the cases with the parallel, perpendicular blood vessel orientations and without blood flow. In these figures we don't show the simulated temperature that is higher than 56 °C, because as we mentioned before it is the threshold value for the tissue necrosis. For the case without blood flow an ellipsoidal shape of lesion with the dimensions 11.7 mm × 2.4 mm × 2.4 mm is obtained. The parallel blood flow tends to reduce the lesion size in axial and radial directions, while the perpendicular blood flow reduces the lesion size only in the radial direction. For the case with a parallel flow the lesion size is reduced from 2.4 to 2.0 mm in the radial direction. The

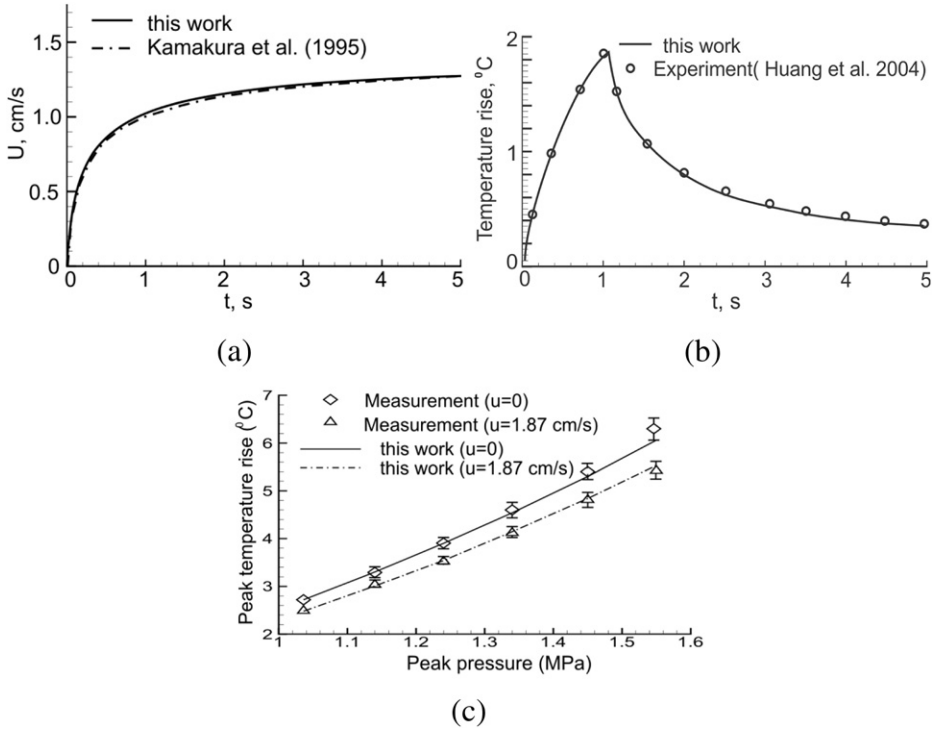

Fig. 5. Validation of the computational model. (a) The currently predicted results are compared with the streaming velocity data of Kamakura et al. [42]; (b) comparison of the simulated focal temperature in a uniform phantom with the experimental data [45]; (c) comparison of the simulated peak temperature rise at the focus (positioned in a phantom material and 0.4 mm from the vessel wall) with the experimental data [45] as a function of pressure for different flow speeds in the vessel.

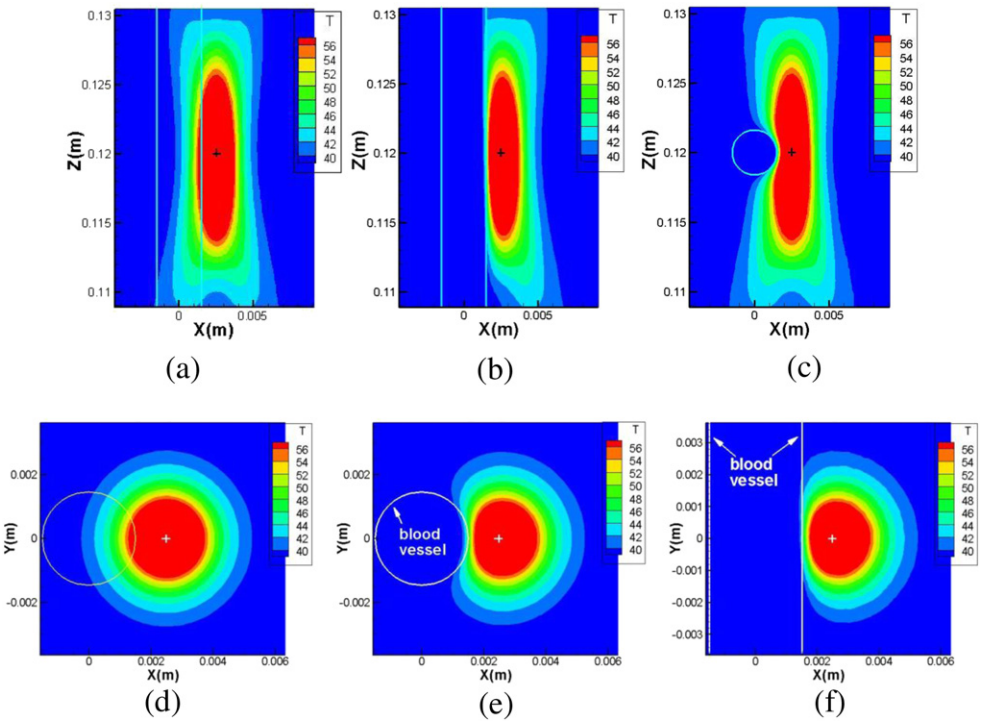

Fig. 6. The predicted temperature contours at $t = 8$ s (immediately after sonication) in liver at the cutting planes $y = 0$ (a, b, c) and $z = 0.12$ m (d, e, f) for the case investigated at $f = 1.0$ MHz and 3.27 MPa pressure at the focal point (0.0025, 0, 0.12), $d = 3$ mm, gap = 1 mm. (a, d) Without blood flow; (b, e) parallel blood flow, $u = 0.13$ m/s; (c, f) perpendicular blood flow, $u = 0.13$ m/s.

distance between the lesion and blood vessel wall is 0.2 mm for the parallel blood flow and 0.25 mm for the perpendicular orientation of blood vessel. This explains why the tissues proximal to blood vessel remain viable. A layer of tissues proximal to the blood vessel receives a smaller thermal dose due to blood cooling. Some studies showed [13,46] that higher focal intensities and smaller exposure times can reduce the distance between the lesion and the blood vessel wall.

In Fig. 7 we can see the temperature profiles computed at $t = 8$ s and $t = 20$ s along the focal axis z and the radial axis x. At $t = 8$ s the peak temperature is 78.8 °C at the focus in the absence of blood flow. If we take into account the blood flow, the temperature at the focal point becomes 75.8 °C for the parallel flow and 75.3 °C for the perpendicular flow. The simulated temperature profile becomes asymmetric in the presence of blood flow. There is a very fast temperature drop near the blood vessel wall. The maximal temperature along the radial axis shifts a length of 0.1 mm from the focal point at $t = 8$ s. At $t = 20$ s, the peak temperature at the focal point is 46.3 °C for the case considering without the blood flow and 42.4 °C for the cases with the parallel and perpendicular blood flows. At $t = 20$ s, in the presence of blood flow the peak temperature shifts a length of 0.9 mm from the focal point along the radial axis. At time $t = 20$ s there is a large discrepancy between the temperature distributions for the cases with and without blood flow. The effect of blood flow cooling increases with the increased treatment time. If destruction of all cells near the blood vessel

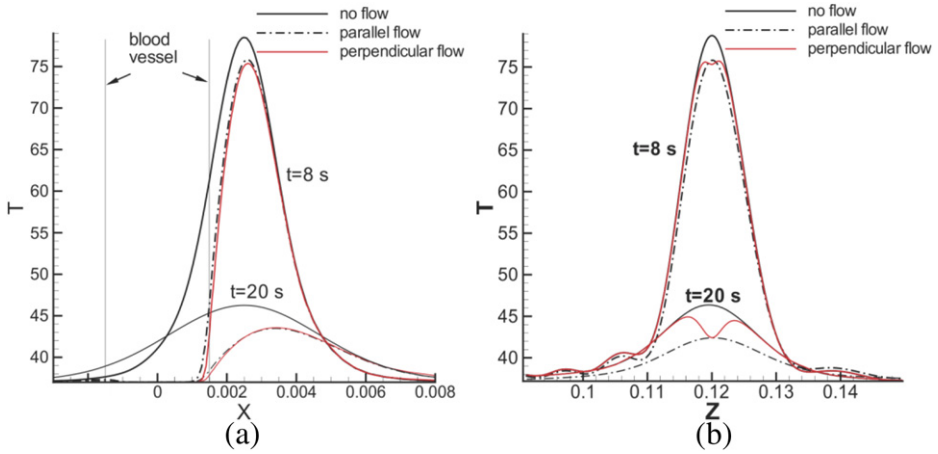

Fig. 7. The predicted temperature distributions at $t = 8$ s and $t = 20$ s along x (axial distance) and z (radial distance) directions for the cases with and without blood flow investigated at $f = 1.0$ MHz.

boundary is necessary, a shorter sonication time with higher power deposition is suggested to minimize the viable region. We have computed the temperature for several distances between the focal point and blood vessel boundary. The calculated results show that the presence of large blood vessel can significantly change the temperature distribution in liver tumor when the distance between the focal point and blood vessel boundary is equal to several millimeters. Next we will study the effect of acoustic streaming on the velocity and temperature distributions in the investigated domain.

3.3. Acoustic streaming buildup

First we will study how the absorbed ultrasound energy can change the velocity distribution in blood vessel. It is interesting to see how the diameter of blood vessel can affect the acoustic streaming profile.

In Fig. 8 we present the z velocity components at the cutting planes $y = 0$ and $z = 0.12$ for two focal point locations in the blood vessel: at the center of blood vessel and on the blood vessel wall. The initial velocity is equal to zero, the diameter of blood vessel is $d = 3$ mm. Acoustic streaming velocity is induced by the absorbed ultrasound energy. We can see that focused ultrasound can induce acoustic streaming velocities up to 12 cm/s. The velocity gradient associated with the acoustic streaming motion is very high, especially, near the boundaries. The point with the maximum velocity is located in the postfocal region owing to the mass flowing out of the focal region. When the focal point is at the center of blood vessel we have the axially flowing blood in the center of the blood vessel and the reverse flow near the boundary region. The total mass flow through any cross section is equal to zero. The velocity increases very fast near the focus. Within 0.2 s the flow becomes steady-state. When the focal point is on the blood vessel wall, there is one large circulation eddy in the blood vessel.

The dependence of the maximum velocity on the blood vessel diameter is presented in Table 2. We found that the peak velocity increases with the increasing blood vessel diameter. For the diameter of blood vessel 3 mm the maximum acoustic streaming velocity is 10 cm/s. For a blood vessel diameter smaller than 2 mm,

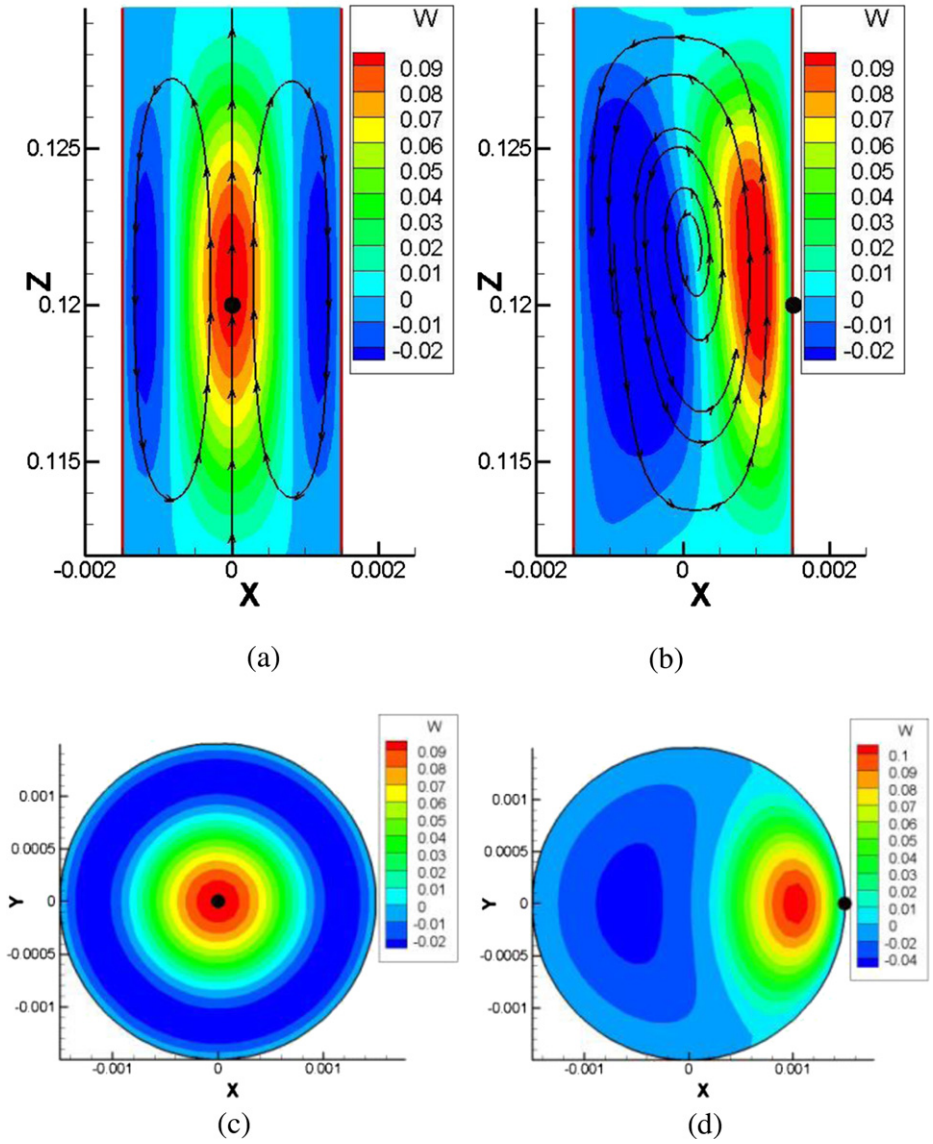

Fig. 8. The simulated streaming profiles at the cutting planes $y = 0$ (a, b) and $z = 0.12$ m (c, d) without the externally applied flow (initial velocity = 0) for two distances between the focal point (circle) and the vessel wall, $d = 3$ mm. (a, c) Focal point is at the center of blood vessel at $x = 0$ m and $z = 0.12$ m; (b, d) focal point is on the blood vessel wall at $x = 0.0015$ m and $z = 0.12$ m.

Table 2
The maximum streaming velocity computed in the blood vessel for two investigated focal point locations. A) Focal point is at the center of blood vessel; B) focal point is on the blood vessel wall.

Diameter, mm	Maximum velocity, m/s (A)	Maximum velocity, m/s (B)
1.0	0.002	0.009
1.4	0.008	0.026
2.0	0.028	0.060
3.0	0.10	0.11
6.0	0.22	0.15

when the focal point is on the blood vessel wall the peak velocity is larger than that for the case with the focal point at the center of blood vessel. In the present study the intensity generated at the focus is 327 W/cm^2. Nowicki et al. showed that acoustic streaming velocity linearly depends on the applied ultrasound power [28]. Increase of the acoustic intensity will cause an increase of acoustic streaming velocity magnitude. At high ultrasound powers nonlinear propagation effects become important, waveform distortion occurs, and higher harmonics are generated. Nonlinear effects lead to an enhanced energy deposition in the focal region, and the acoustic streaming effect is strongly enlarged in this case.

In Fig. 9 the simulated velocity profiles w at the focal plane is presented for different distances between the focal point and the blood vessel center for the blood vessel diameters $d = 1.4$ and 3 mm. The largest velocity magnitude 0.12 m/s for the blood vessel diameter $d = 3$ mm is obtained for the case when the focal point is at $x = 0.5$ mm. When the distance between the blood vessel wall and focal point is 0.5 mm (focal point is in liver at $x = 2.0$ mm), the maximum velocity is 0.047 cm/s. Increase of the distance between the focal point and blood vessel wall results in a decrease of the acoustic streaming velocity. Increasing the blood vessel diameter causes an increase of the acoustic streaming velocity and, consequently, an increase of the blood flow cooling. In the next sections we will see that the effect of acoustic streaming on the temperature elevation becomes more pronounced for larger blood vessel diameters.

In Fig. 10 the simulated velocity profiles are presented for the cases with and without acoustic streaming for the blood vessel diameter $d = 3$ mm. We study the blood flow velocities 0.016 m/s (corresponding to the velocity in vein with $d = 3$ mm) and 0.13 m/s (artery) for $d = 3$ mm. When we take into account the acoustic streaming effect, blood flow becomes asymmetric. If the initial velocity is increased, the acoustic streaming becomes less important. For the presented cases we get a larger velocity gradient near the blood vessel boundary, when the acoustic streaming effect is taken into account. This will increase the blood flow cooling and decrease the temperature rise.

3.4. Effect of acoustic streaming on the temperature distribution

In Figs. 11 and 12 we present the temperature difference at $t = 8$ s (exposure time = 8 s) for the cases investigated with and without inclusion of acoustic streaming for the parallel (Fig. 11) and perpendicular (Fig. 12) blood flow orientations. The distance between the focal point and blood vessel wall (the gap) is 0.5 mm, the diameter of blood vessel is 3 mm. The blood flow velocity is 0.016 m/s (vein).

For the case of parallel flow the largest temperature difference is found at the point close to the blood vessel wall and the magnitude is about 8 °C (Fig. 11(c)). On the blood vessel wall (0.0015, 0, 0.12) the temperature rise is 20.2 °C without acoustic streaming effect and 13.1 °C with acoustic streaming effect. This means that as we don't take into account acoustic streaming the temperature is overestimated by 54%. Inside the blood vessel the temperature rise for the cases investigated with and without inclusion of acoustic streaming can differ by three times. At the location with the distance 1.5 mm from the blood vessel wall the difference between the cases investigated with and without acoustic streaming effect is 3%.

For the case of perpendicular flow (Fig. 12) the largest temperature difference is about 4 °C (8 °C for parallel flow) and is located close to the blood vessel wall, but is shifted in the direction of blood flow. On the blood vessel wall (0.0015, 0, 0.12) the temperature difference for the cases with and without acoustic streaming is 3 °C (27%). In Figs. 11 and 12 we can see that the effect of acoustic streaming at the distance about 1.5 mm from the blood vessel wall is important for both parallel and perpendicular blood vessel orientations. The region close to the blood vessel wall is very important in the treatment planning. As a result, the effect of acoustic streaming should be taken into account. However for the case of perpendicular flow the effect of acoustic streaming is less pronounced comparing with the perpendicular flow case.

For the vein with the diameter $d = 1.4$ mm (Fig. 13) the largest temperature difference for the cases with and without acoustic streaming is about 5 °C. The blood flow velocity is 0.01 m/s. At the point on the blood vessel wall (0.0007, 0, 0.12) the temperature rise is 22.7 °C without acoustic streaming effect and 18.5 °C with acoustic streaming effect (23% difference). The effect of acoustic streaming on the temperature elevation is more pronounced for the blood vessels with larger diameter.

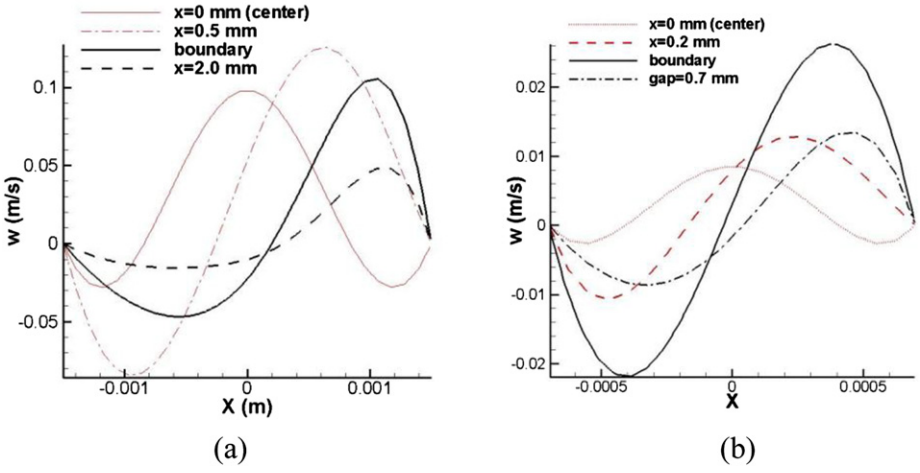

Fig. 9. The simulated velocity profiles w (x; $y = 0$; $z = 0.12$ m) at the focal plane for different distances between the focal point and blood vessel center. (a) $d = 3$ mm; (b) $d = 1.4$ mm.

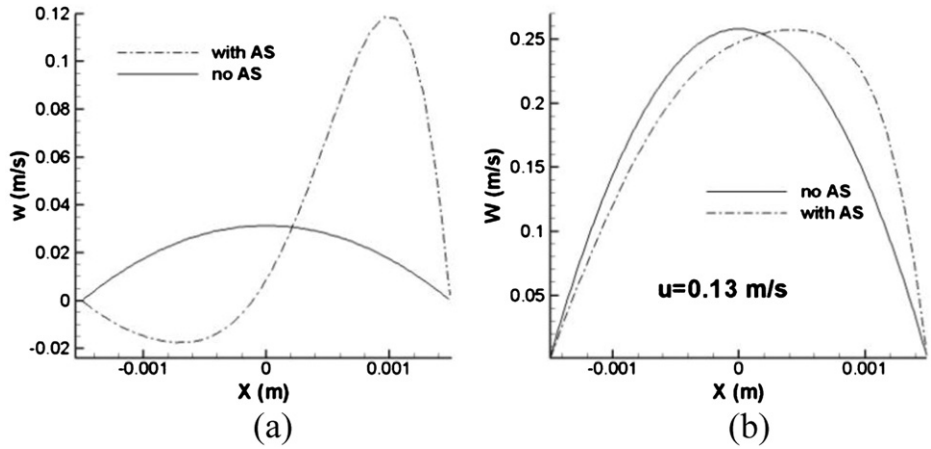

Fig. 10. The simulated velocity profiles w at the focal plane for the cases with and without acoustic streaming. Focal point is located on the vessel wall, $d = 3$ mm. (a) inlet average velocity is 0.016 m/s (vein); (b) inlet average velocity is 0.13 m/s (artery).

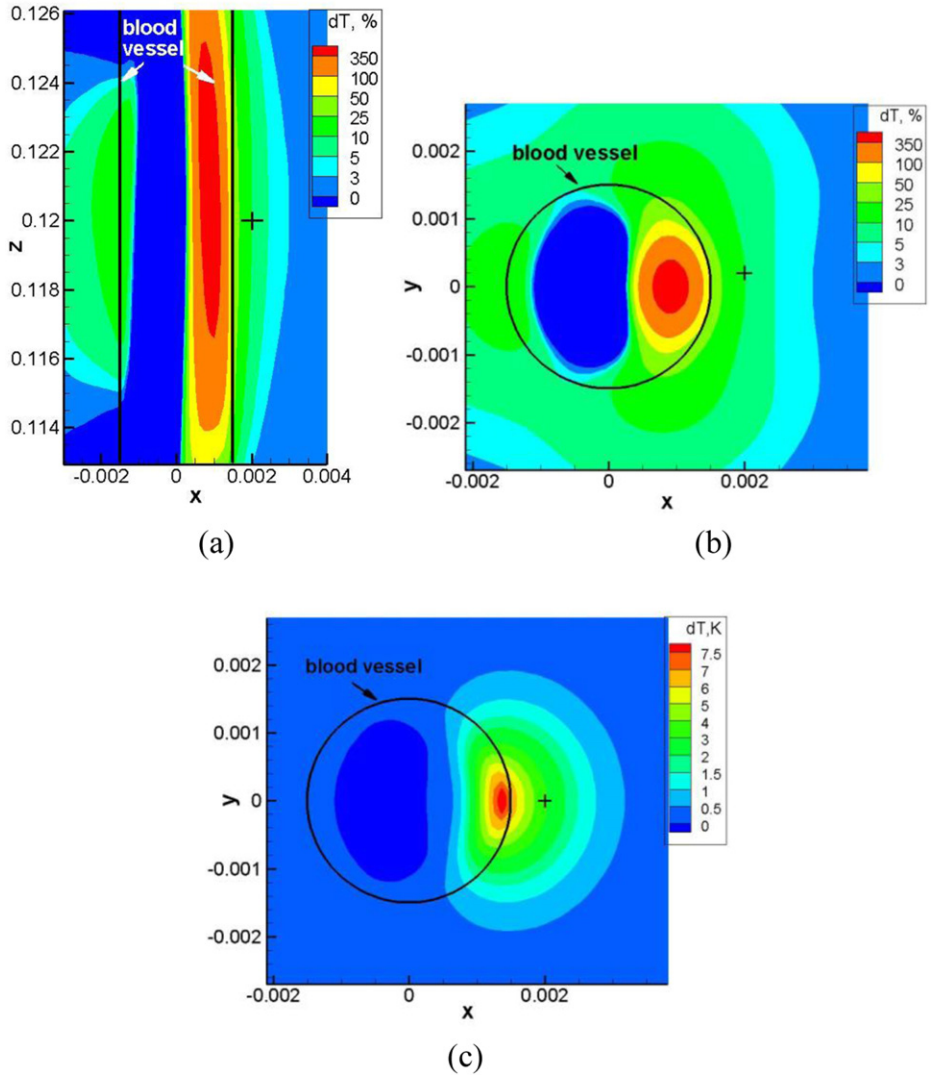

Fig. 11. The temperature difference at $t = 8$ s for the cases with and without acoustic streaming effect, gap = 0.5 mm, $d = 3$ mm, blood flow velocity is 0.016 m/s (vein), cross (+) denotes the focal point. (a) The relative temperature difference at the cutting plane $y = 0$; (b) the relative temperature difference at the cutting plane $z = 0.12$; (c) the absolute temperature difference at the cutting plane $z = 0.12$.

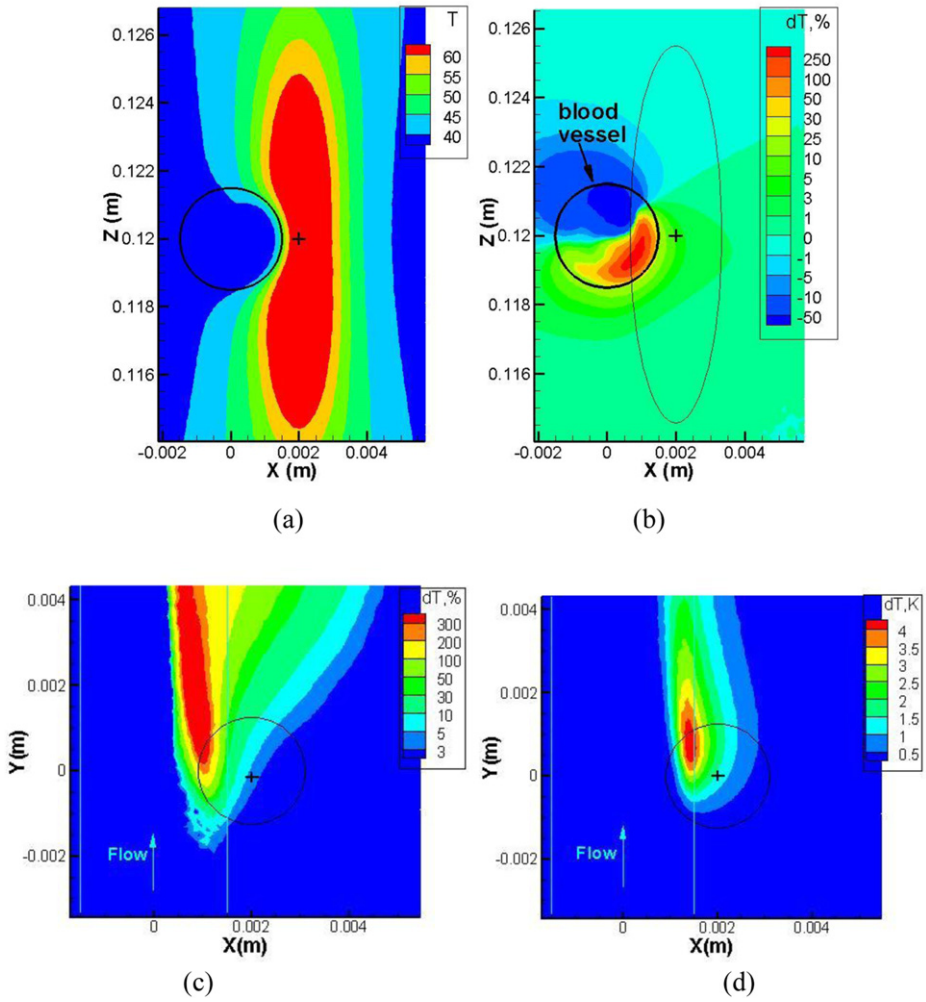

Fig. 12. The predicted temperature and temperature difference at $t = 8$ s for the cases with and without acoustic streaming effect for the perpendicular flow orientation, gap = 0.5 mm, $d = 3$ mm, blood flow velocity is 0.016 m/s (vein), cross (+) denotes the focal point. (a) The temperature at the cutting plane $y = 0$; (b) the relative temperature difference at the cutting plane $y = 0$; (c) the relative temperature difference at the cutting plane $z = 0.12$; (d) the absolute temperature difference at the cutting plane $z = 0.12$.

The predicted temperatures plotted as the function of initial velocity (m/s) for the cases with and without acoustic streaming effect at the focal point and on the blood vessel wall $(d/2, 0, 0.12)$ are shown in Fig. 14 for two blood vessel diameters $d = 1.4$ mm and $d = 3$ mm. The inlet average velocities $u = 0.01$ m/s and $u = 0.08$ m/s correspond to the velocity in vein and artery with the diameter $d = 1.4$ mm. For the case with the inlet velocity $u = 0.01$ m/s the temperature differences for the cases considered with and without acoustic streaming are 65% for $d = 3$ mm and 23% for $d = 1.4$ mm on the blood vessel wall. For the case with the inlet velocity $u = 0.08$ m/s (corresponds to the velocity in artery with $d = 1.4$ mm) the temperature difference is 23% and 6.5% for the diameters $d = 3$ mm and $d = 1.4$ mm, correspondingly. At the focal point the temperature rise difference for the diameter $d = 3$ mm for the cases considered with and without acoustic streaming is 10% and 2.4% for the inlet average inlet velocity $u = 0.016$ m/s (vein) and 0.13 m/s (artery), correspondingly. For large diameters ($d = 3$ mm) the effect of acoustic streaming is more pronounced. When the inlet average velocity is increased, the effect of acoustic streaming decreases.

3.5. Effect of acoustic streaming on the lesion size

In Fig. 15 we present the predicted lesion boundaries in liver for the cases with and without acoustic streaming effect for parallel and perpendicular blood vessel orientations. The lesion size for the case of blood flow velocity 0.016 m/s is calculated based on the thermal-dose threshold value of 240 min. When taking into account the acoustic streaming effect, the lesion size can be reduced by 22% for the parallel flow and 2% for the perpendicular flow. When the distance between the focal point and the blood vessel boundary becomes smaller, the effect of acoustic streaming becomes more pronounced. The simulated results for the parallel flow (Fig. 15a, b) without inclusion of acoustic streaming effect show that tissues close to blood vessel can be completely ablated. However, if the effect of acoustic streaming is taken into account, a thin layer of tissue (0.09 mm) close to blood vessel remains viable. So the effect of acoustic streaming cannot be neglected in the treatment planning. For the case of perpendicular flow the layer of viable region differs from 0.08 mm for the case without acoustic streaming to 0.14 mm when acoustic streaming effect is taken into account. Zhang et al. [10] suggested that HIFU combined with chemotherapy can be used to increase the efficiency of the treatment and prolong the survival.

The simulated ablated tumor volumes, which vary with the initial velocity, for the cases with and without acoustic streaming are presented in Fig. 16. The blood vessel is parallel to the acoustic axis. The distances 0.5 mm and 0.7 mm between the blood vessel boundary and focal point are considered. The diameter of blood

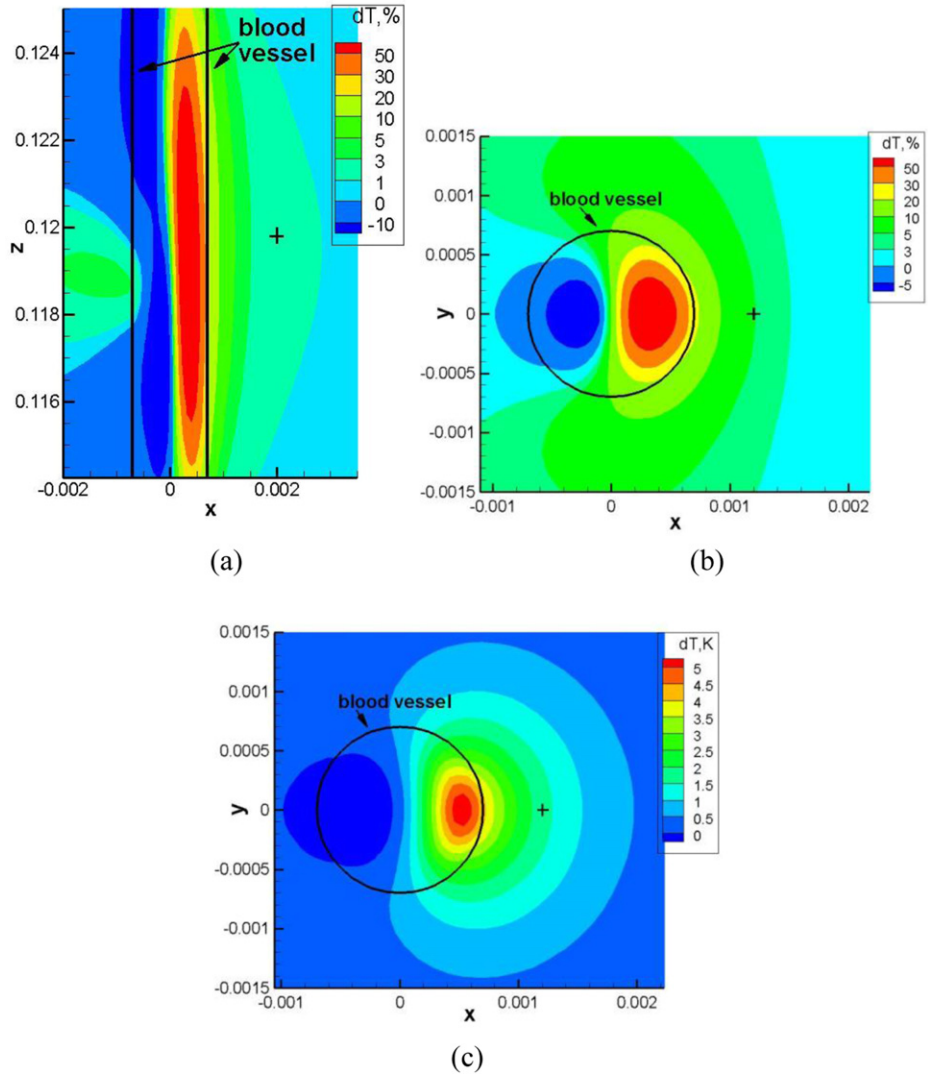

Fig. 13. The relative temperature difference at $t = 8$ s for the cases with and without acoustic streaming effect, gap = 0.5 mm, $d = 1.4$ mm, blood flow velocity is 0.01 m/s (vein), cross (+) denotes the focal point. (a) The relative temperature difference at the cutting plane $y = 0$; (b) the relative temperature difference at the cutting plane $z = 0.12$; (c) the absolute temperature difference at the cutting plane $z = 0.12$.

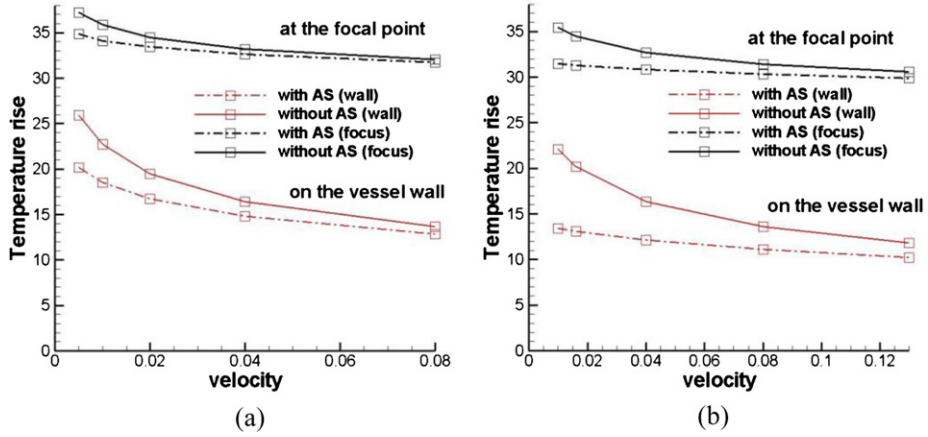

Fig. 14. The predicted temperatures as the function of inlet average velocity (m/s) for the cases with and without acoustic streaming effect at the focal point and on the blood vessel wall (d/2, 0, 0.12), $t = 8$ s, gap = 0.5 mm. (a) $d = 1.4$ mm; (b) $d = 3$ mm.

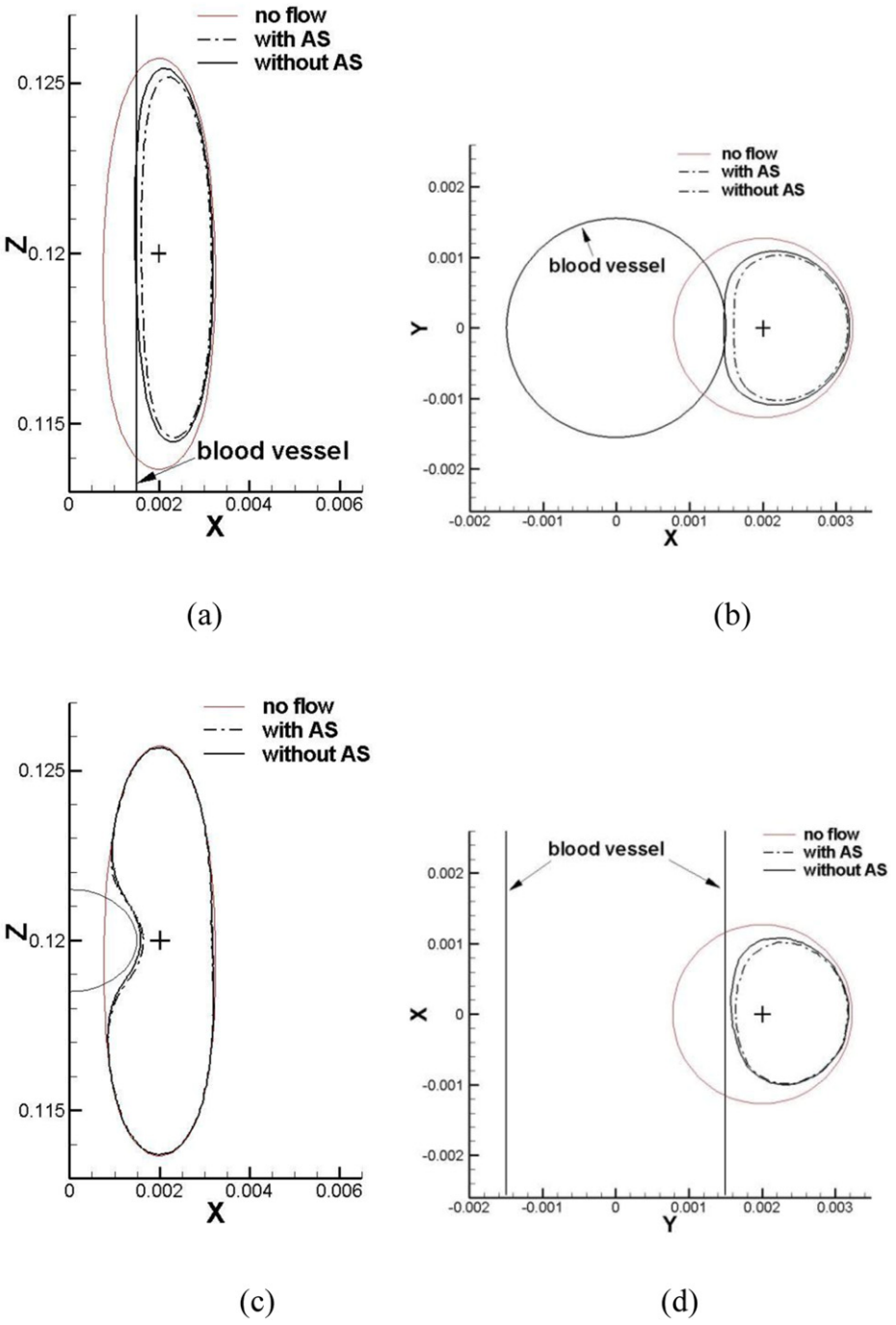

Fig. 15. The predicted lesion shapes in liver for the cases with and without acoustic streaming effect for the parallel (a, b) and for the perpendicular (c, d) blood flow, $t = 8$ s, gap = 0.5 mm, blood flow velocity is 0.016 m/s. (a) At the cutting plane $y = 0$; (b) at the cutting plane $z = 0.12$; (c) at the cutting plane $y = 0$; (d) at the cutting plane $z = 0.12$.

vessel is $d = 3$ mm. When we increase the velocity from 0.01 m/s to 0.04 m/s, the volume calculated for the case without taking into account the acoustic streaming effect is decreased by an amount of 25%. When increasing the velocity from 0.04 m/s to 0.08 m/s the difference of the volumes calculated without taking into account the acoustic streaming effect is only 12.5%. A further increase of the velocity will decrease the ablated volume by only a small amount.

In Fig. 16 we can see that inclusion of acoustic streaming into the current analysis decreases the ablated tumor volume. At the velocity 0.01 m/s the volume difference for the cases with and without acoustic streaming is equal to 28% for the gap 0.5 mm and 14% for the gap 0.7 mm. With the increasing initial velocity the difference decreases accordingly. For the case with the velocity 0.13 m/s the difference in volumes is only 3% and 1.4% for the gaps of 0.5 mm and 0.7 mm, correspondingly. Increasing the gap from 0.5 mm to 0.7 mm results in an increased lesion volume. For the case of larger gaps the importance of acoustic streaming effect becomes smaller. For the gap of 0.9 mm the predicted difference of volumes for the cases with and without acoustic streaming is equal to 5% for the gap = 0.5 mm and velocity $u = 0.016$ m/s (vein). As we can see in Fig. 15, inclusion of acoustic streaming can considerably change the distance between the lesion and the blood vessel wall.

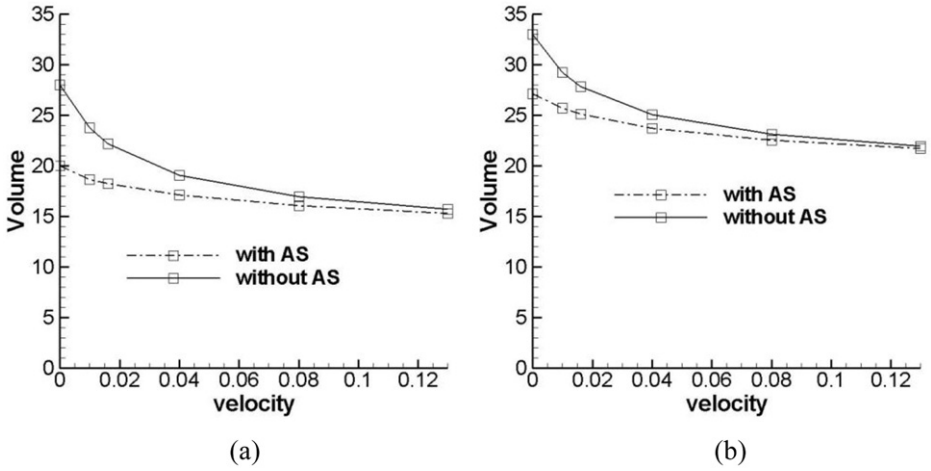

Fig. 16. The simulated ablated tumor volumes (mm^3) as the function of inlet average velocity (m/s) for the cases with and without acoustic streaming, $d = 3$ mm. (a) gap = 0.5 mm; (b) gap = 0.7 mm.

The predicted results show that acoustic streaming can affect the lesion size, when the distance between the focal point and blood vessel wall becomes less than 1 mm. The transducer used in the simulation has a half-pressure amplitude width of 1.1 mm. So when the blood vessel is located within the half-pressure amplitude width, the acoustic streaming effect is important.

4. Conclusion

A three dimensional physical model is proposed in this study to perform the current HIFU simulation. This physical model takes into account the convective cooling in large blood vessel and the perfusion due to capillary flows. Convective cooling in large blood vessel was shown to be able to reduce the temperature near large blood vessel. Acoustic streaming was also included in the simulation model. The effect of acoustic streaming was underestimated previously. For the diameter of blood vessel 3 mm the maximum acoustic streaming velocity is 12 cm/s. Due to the enhanced cooling effect by acoustic streaming, the temperature rise near the blood vessel boundary is much smaller than the value predicted without taking into account the acoustic streaming effect. The predicted temperature difference for the cases considered with and without acoustic streaming effect is 54% on the blood vessel wall for the diameter of blood vessel 3 mm. For the smaller diameter of blood vessel the effects of blood flow cooling and acoustic streaming on the temperature distribution become smaller (Fig. 14). Two blood vessel orientations were studied: parallel and perpendicular. When the blood vessel is parallel to the acoustic axis, the effects of acoustic streaming and the blood flow cooling on the temperature distribution and lesion size are more pronounced, comparing that for the case with perpendicular blood vessel orientation.

It was shown that acoustic streaming can affect the lesion size and the shape generated by ultrasound. This demonstrates the necessity of taking both of the convective cooling and acoustic streaming effects into account for a simulation involving a large blood vessel, when the tumor is proximal to the thermally significant blood vessel. Two major conclusions drawn from the current study are summarized below. Firstly, if the distance between the ultrasound beam and blood vessel is equal to several mm (2–3 mm), the convective cooling should be taken into account and the homogenization assumption becomes no longer acceptable. Secondly, acoustic streaming effect becomes important when the distance between the focal point and blood vessel wall is less than 1 mm. These results can be further used to construct a surgical planning platform for the non-invasive HIFU tumor ablating therapy in real liver geometry on the basis of the MRI image.

Acknowledgements

The authors would like to acknowledge the financial support from the Center of Advanced Study in Theoretical Science (CASTS). The authors also would like to thank Dr. I. Kuo from National Health Research Institutes, Taiwan for assistance with pressure measurements.

References

[1] Y.F. Zhou, High intensity focused ultrasound in clinical tumor ablation, World J. Clin. Oncol. 2 (2011) 8–27.
[2] T.A. Leslie, J.E. Kennedy, High intensity focused ultrasound in the treatment of abdominal and gynaecological diseases, Int. J. Hyperth. 23 (2007) 173–182.
[3] O. Al-Bataineha, J. Jenneb, P. Huberb, Clinical and future applications of high intensity focused ultrasound in cancer, Cancer Treat. Rev. 38 (5) (2012) 346–353.
[4] N.T. Wright, J.D. Humphrey, Denaturation of collagen via heating: an irreversible rate process, Annu. Rev. Biomed. Eng. 4 (2002) 109–128.
[5] V.A. Khokhlova, M.R. Bailey, J.A. Reed, B.W. Cunitz, P.J. Kaczkowski, L.A. Crum, Effects of nonlinear propagation, cavitation and boiling in lesion formation by high intensity focused ultrasound in a gel phantom, J. Acoust. Soc. Am. 119 (3) (2006) 1834–1848.
[6] W.S. Chen, C. Lafon, T.J. Matula, S. Vaezy, L.A. Crum, Mechanisms of lesion formation in high intensity focused ultrasound therapy, Acoust. Res. Lett. Online 4 (2) (2003) 41–46.
[7] J.S. Huang, D.A. Gervais, P.R. Mueller, Radiofrequency ablation: review of mechanism, indications, technique, and results, Chin. J. Radiol. 26 (2001) 119–134.
[8] M. Thiriet, Biology and Mechanics of Blood Flows. Part II: Mechanics and Medical Aspects, Springer, New York, 2008.
[9] D.S.K. Lu, S.S. Raman, D.J. Vodopich, M. Wang, J. Sayre, C. Lassman, Effect of vessel size on creation of hepatic radiofrequency lesions in pigs: assessment of the "heat sink" effect, Am. J. Roentgenol. 178 (2002) 47–51.
[10] L. Zhang, H. Zhu, C. Jin, K. Zhou, K. Li, H. Su, W. Chen, J. Bai, Z. Wang, High-intensity focused ultrasound (HIFU): effective and safe therapy for hepatocellular carcinoma adjacent to major hepatic veins, Eur. Radiol. 19 (2009) 437–445.
[11] H.H. Pennes, Analysis of tissue and arterial blood temperature in the resting human forearm, J. Appl. Physiol. 1 (2) (1948) 93–122.
[12] M.C. Kolios, M.D. Sherar, J.W. Hunt, Large blood vessel cooling in heated tissues: a numerical study, Phys. Med. Biol. 40 (1995) 477–494.
[13] M.C. Kolios, M.D. Sherar, J.W. Hunt, Blood flow cooling and ultrasonic lesion formation, Med. Phys. 23 (7) (1996) 1287–1298.
[14] P. Hariharan, M.R. Myers, R.K. Banerjee, HIFU procedures at moderate intensities - effect of large blood vessels, Phys. Med. Biol. 52 (12) (2007) 3493–3513.
[15] T.C. Shih, T.L. Horng, H.W. Huang, K.C. Ju, T.C. Huang, P.Y. Chen, Y.J. Ho, W.L. Lin, Numerical analysis of coupled effects of pulsatile blood flow and thermal relaxation time during thermal therapy, Int. J. Heat Mass Transf. 55 (2012) 3763–3773.

[16] T.W.H. Sheu, M.A. Solovchuk, A.W.J. Chen, M. Thiriet, On an acoustics-thermal-fluid coupling model for the prediction of temperature elevation in liver tumor, Int. J. Heat Mass Transf. 54 (17–18) (2011) 4117–4126.
[17] F.P. Curra, P.D. Mourad, V.A. Khokhlova, R.O. Cleveland, L.A. Crum, Numerical simulations of heating patterns and tissue temperature response due to high-intensity focused ultrasound, IEEE Trans. Ultrason. Ferroelectr. Freq. Control 47 (2000) 1077–1089.
[18] K.R. Nightingale, P.J. Kornguth, W.F. Walker, B.A. McDermott, G.E. Trahey, A novel ultrasonic technique for differentiating cysts from solid lesions: preliminary results in the breast, Ultrasound Med. Biol. 21 (1995) 745–751.
[19] P. Hariharan, M.R. Myers, R.A. Robinson, S.H. Maruvada, J. Sliwa, R.K. Banerjee, Characterization of high intensity focused ultrasound transducers using acoustic streaming, J. Acoust. Soc. Am. 123 (3) (2008) 1706–1719.
[20] J. Friend, L.Y. Yeo, Microscale acoustofluidics: microfluidics driven via acoustics and ultrasonics, Rev. Mod. Phys. 83 (2011) 647–704.
[21] J.W.S. Rayleigh, On the circulation of air observed in Kundt's tubes, and on some allied acoustical problems, Philos. Trans. R. Soc. Lond. 175 (1884) 1–21.
[22] C. Eckart, Vortices and streams caused by sound waves, Phys. Rev. 73 (1948) 68–76.
[23] A. Perelomova, Development of linear projecting in studies of non-linear flow. Acoustic heating induced by non-periodic sound, Phys. Let. A 357 (2006) 42–47.
[24] O.V. Rudenko, S.I. Soluyan, Theoretical Foundation of Nonlinear Acoustics, Plenum, New York, 1977. (Chapter 8).
[25] W.L. Nyborg, Acoustic streaming, in: M.F. Hamilton, D.T. Blackstock (Eds.), Nonlinear Acoustics, Academic, San Diego, 1998. (Chapter 7).
[26] X. Shi, R.W. Martin, S. Vaezy, L.A. Crum, Quantitative investigation of acoustic streaming in blood, J. Acoust. Soc. Am. 111 (2) (2002) 1110–1121.
[27] H.C. Starritt, F.A. Duck, V.F. Humphrey, An experimental investigation of streaming in pulsed diagnostic ultrasound beams, Ultrasound Med. Biol. 15 (1989) 363–373.
[28] A. Nowicki, W. Secomski, J. Wojcik, Acoustic streaming: comparison of low-amplitude linear model with streaming velocities measured by 32-MHz Doppler, Ultrasound Med. Biol. 23 (1997) 783–791.
[29] C.C. Coussios, R.A. Roy, Applications of acoustics and cavitation to non-invasive therapy and drug delivery, Annu. Rev. Fluid Mech. 40 (2008) 395–420.
[30] E. VanBavel, Effects of shear stress on endothelial cells: possible relevance for ultrasound applications, Prog. Biophys. Mol. Biol. 93 (2007) 374–383.
[31] H.C. Starritt, C.L. Hoad, F.A. Duck, D.K. Nassiri, I.R. Summers, W. Vennart, Measurement of acoustic streaming using magnetic resonance, Ultrasound Med. Biol. 26 (2000) 321–333.
[32] J. Wu, A.J. Winkler, T.P. O'Neill, Effect of acoustic streaming on ultrasonic heating, Ultrasound Med. Biol. 20 (1994) 195–201.
[33] C.N. Layman, I.M. Sou, R. Bartak, C. Ray, J.S. Allen, Characterization of acoustic streaming and heating using synchronized infrared thermography and particle image velocimetry, Ultrason. Sonochem. 18 (2011) 1258–1261.
[34] F.J. Trujillo, K. Knoerzer, Modeling the acoustic field and streaming induced by an ultrasonic horn reactor, in: K. Knoerzer, P. Juliano, P. Roupas, C. Versteeg (Eds.), Innovative Food Processing Technologies: Advances in Multiphysics Simulation, John Wiley & Sons, 2011, pp. 233–264. (Chapter 12).
[35] M.F. Hamilton, C.L. Morfey, Model equations, in: M.F. Hamilton, D.T. Blackstock (Eds.), Nonlinear Acoustics, Academic, San Diego, 1998. (Chapter 3).
[36] M. Bailey, V. Khokhlova, O. Sapozhnikov, S. Kargl, L. Crum, Physical mechanism of the therapeutic effect of ultrasound (a review), Acoust. Phys. 49 (4) (2003) 369–388.
[37] A.D. Pierce, Acoustics. An Introduction to Its Physical Principles and Applications, McGraw-Hill, New York, 1981.
[38] H.T. O'Neil, Theory of focusing radiators, J. Acoust. Soc. Am. 21 (5) (1949) 516–526.
[39] M.S. Canney, M.R. Bailey, L.A. Crum, V.A. Khokhlova, O.A. Sapozhnikov, Acoustic characterization of high intensity focused ultrasound fields: a combined measurement and modeling approach, J. Acoust. Soc. Am. 124 (4) (2008) 2406–2420.
[40] I.M. Hallaj, R.O. Cleveland, FDTD simulation of finite-amplitude pressure and temperature fields for biomedical ultrasound, J. Acoust. Soc. Am. 105 (5) (1999) L7–L12.
[41] S.A. Sapareto, W.C. Dewey, Thermal dose determination in cancer therapy, Int. J. Radiat. Oncol. Biol. Phys. 10 (6) (1984) 787–800.
[42] T. Kamakura, M. Matsuda, Y. Kumamoto, M.A. Breazeale, Acoustic streaming induced in focused Gaussian beams, J. Acoust. Soc. Am. 97 (1995) 2740–2746.
[43] F.A. Duck, Physical Property of Tissues – A Comprehensive Reference Book, Academic, London, 1990.
[44] H.R. Yazdi, H. Sotoudeh, Assessment of normal doppler parameters of portal vein and hepatic artery in 37 healthy Iranian volunteers, Iran. J. Radiol. 3 (2006) 213–216.
[45] J. Huang, R.G. Holt, R.O. Cleveland, R.A. Roy, Experimental validation of a tractable medical model for focused ultrasound heating in flow-through tissue phantoms, J. Acoust. Soc. Am. 116 (4) (2004) 2451–2458.
[46] M.A. Solovchuk, T.W.H. Sheu, W.L. Lin, I. Kuo, M. Thiriet, Simulation study on acoustic streaming and convective cooling in blood vessels during a high-intensity focused ultrasound thermal ablation, Int. J. Heat Mass Transf. 55 (4) (2012) 1261–1270.
[47] M.A. Solovchuk, T.W.H. Sheu, M. Thiriet, The effects of acoustic streaming on the temperature distribution during focused ultrasound therapy, AIP Conf. Proc. 1433 (2012) 589–592.
[48] M.A. Solovchuk, T.W.H. Sheu, M. Thiriet, Effects of acoustic nonlinearity and blood flow cooling during HIFU treatment, AIP Conf. Proc. 1503 (2012) 83–88.
[49] H.P. Rani, Tony W.H. Sheu, T.M. Chang, P.C. Liang, Numerical investigation on non-Newtonian microcirculatory blood flow in hepatic lobule, J. Biomech. 39 (2005) 551–563.
[50] T.L. Horng, W.L. Lin, C.T. Liauh, T.C. Shih, Effects of pulsatile blood flow in large vessels on thermal dose distribution during thermal therapy, Med. Phys. 34 (2007) 1312–1320.
[51] J.W. Hand, Ultrasound hyperthermia and the prediction of heating, in: F.A. Duck, A.C. Baker, H.C. Starritt (Eds.), Ultrasound in Medicine, Institute of Physics Publishing, Bristol, 1998. (Chapter 8).